Frequency-shifting-based algebraic approach to extended state observer design

Kasac, Josip; Pender, Antonia; Pranjic, Marko; Kotarski, Denis

Source / Izvornik: **Asian Journal of Control, 2021, 23, 2171 - 2184**

Journal article, Accepted version
Rad u časopisu, Završna verzija rukopisa prihvaćena za objavljivanje (postprint)

https://doi.org/10.1002/asjc.2516

Permanent link / Trajna poveznica: https://urn.nsk.hr/urn:nbn:hr:235:494747

Rights / Prava: In copyright / Zaštićeno autorskim pravom.

Download date / Datum preuzimanja: **2024-07-14**

Repository / Repozitorij:

Repository of Faculty of Mechanical Engineering and Naval Architecture University of Zagreb

Asian Journal of Control, Vol. 13, No. 1, pp. 1–14, January 2011
Published online in Wiley InterScience (www.interscience.wiley.com) DOI: 10.1002/asjc.273

Frequency-shifting-based algebraic approach to extended state observer design

Josip Kasac, Antonia Pender, Marko Pranjic, and Denis Kotarski

ABSTRACT

In this paper, a frequency-shifting-based (FSB) algebraic approach to the extended state observer (ESO) design is proposed. The proposed algebraic approach provides almost instantaneous convergence towards the exact values of the system states and disturbances. The main benefit of the proposed approach is the elimination of the peaking phenomenon, which is inevitable in the case of the conventional observer design. In comparison with the linear ESO, the proposed algebraic ESO is less sensitive to the choice of the observer bandwidth, and it is more robust to the measurement noise. The simulation and experimental results illustrate the efficiency of the proposed algebraic approach in comparison with the linear ESO.

Key Words: active disturbance rejection control, extended state observer, algebraic state estimation, peaking phenomenon

I. INTRODUCTION

Control of nonlinear systems with unknown dynamics and partially measurable state variables in the presence of external disturbances is still a topic of active research and a large number of approaches have been proposed in the literature. The active disturbance rejection control (ADRC) emerged relatively recently as a promising methodology for the output control of uncertain systems with unknown external disturbances [1, 2, 3]. The main idea of the ADRC is that the model uncertainty and external disturbances are aggregated to one total disturbance, and the extended state observer (ESO) is used to estimate the system state and total disturbance, which is treated as an extended system state [4, 5]. The estimated extended state is then used in the feedback controller to compensate the unknown total disturbance.

The ADRC has been successfully used to control various uncertain dynamic systems involving the speed control of synchronous motor [6], control of pneumatic actuators [7], control of flexible wing unmanned aerial vehicle [8], control of the hovercraft vessel [9], etc. Also, it has been successfully implemented for the control of systems with the input time-delay [10].

The ESO is the key component of the ADRC methodology, and its estimation accuracy determines the control performance of the closed-loop system [11, 12, 13]. The conventional ESO has limited accuracy and phase delay in the estimation of the system state, which deteriorates the control performance of the ADRC system. Better accuracy and performance improvement can be achieved by increasing the observer gains [14].

However, the high observer gains may lead to the so-called peaking phenomenon, i.e., the appearance of high amplitude oscillations in the transient response of the estimated variables. If the observer is a component of an output feedback system, it results in large control input, which may not be feasible in a real actuator. The peaking phenomenon significantly deteriorates the control performances and could even destabilize the closed-loop nonlinear system. Another disadvantage of the high-gain observers is the limited robustness

Josip Kasac is with the University of Zagreb, Faculty of Mechanical Engineering and Naval Architecture, I. Lucica 5, 10000 Zagreb, Croatia (e-mail: jkasac@fsb.hr).
Antonia Pender is with the University of Applied Sciences in Zagreb, Vrbik 8, Zagreb, Croatia (e-mail: apender@tvz.hr).
Marko Pranjic is with the Karlovac University of Applied Sciences, Karlovac, Croatia (e-mail: marko.pranjic111@gmail.com)
Denis Kotarski is with the Karlovac University of Applied Sciences, Karlovac, Croatia (e-mail: denis.kotarski@vuka.hr)
Antonia Pender is corresponding author.

© 2011 John Wiley and Sons Asia Pte Ltd and Chinese Automatic Control Society
Prepared using asjcauth.cls *[Version: 2008/07/07 v1.00]*

against measurement noise. Hence, the conventional disturbance observer tuning is always a compromise between estimation quality and noise sensitivity.

The peaking phenomenon in high-gain observers has been addressed in several papers. In [15, 16, 17] saturation functions are used to mitigate the peaking in state estimation. In [18] the time-varying gain ESO is presented, with gain value slowly increasing from a small initial value to its maximal value. The time-varying gain methods reduce the peaking phenomenon caused by the constant high gain. A nonlinear non-smooth function is used in [19] for the ESO design to ensure the smaller peaking values of the estimated states. In [20] the reset observers are used to alleviate the peaking phenomenon. Note that the mentioned approaches provide only a reduction of the peaking phenomenon, but not its complete elimination. Also, the proposed observers provide asymptotic convergence of the estimated states.

A promising approach to improve the ESO performances is the state estimation based on the algebraic methodology [21, 22]. The algebraic estimation method provides determination of the system state in the form of an exact algebraic expression which depends only on measurable input and output variables. Unlike traditional methods, the algebraic estimator is non-asymptotic: the convergence towards the exact values of the system states is almost instantaneous. The algebraic methods have been applied mostly to the online parameter identification [21, 23, 24] and to the state estimation [25, 26, 27]. In [28], the algebraic method is applied for the derivative estimation of noisy signals.

The main problem of the conventional algebraic estimation methods is the inherent instability of the state-space realization of the estimator filters. Since the estimator variables are unbounded, an additional periodic resetting mechanism is necessary to ensure the boundedness of the state variables [29]. The problem of the inherent instability of the conventional algebraic estimators is resolved in [30] in the case of the online parameter identification of linear systems of arbitrary order, and in [31] in the case of second-order system state estimation. In [32], a new stable algebraic approach to the online signal derivatives estimation is proposed. The proposed frequency-shifting-based (FSB) algebraic approach provides stable online parameters and state estimation without needs for periodic re-initialization.

In [31] the FSB algebraic approach is applied to the state estimation of the second-order system in the case without external disturbances. In this paper, the FSB algebraic approach is proposed for the design of the ESO for the unknown nonlinear second-order systems with external disturbances. The proposed third-order FSB algebraic observer provides the nonasymptotic estimation of the system position, velocity and the total disturbance. In comparison with the previous methods which provides just a reduction of the peaking phenomenon, the main contribution of this article is design of the stable algebraic ESO which provides its complete elimination. The second contribution is the improvement of the closed-loop system response of the ADRC based on algebraic ESO because the nonasymptotic convergence does not depend on the observer parameters.

The rest of the paper is organized as follows. The ADRC method based on linear ESO is presented in Section II. The frequency-shifting-based algebraic approach to the ESO design is presented in Section III. The comparison with linear ESO is considered in Section IV. The simulation and experimental results are presented in Section V and Section VI, respectively. Finally, the concluding remarks are emphasized in Section VII.

II. ADRC BASED ON LINEAR ESO

In this section, a brief review of the linear ESO is presented for the purpose of comparison with the proposed algebraic ESO.

Consider a single input-single output nonlinear second-order dynamic system described by

$$\ddot{y} = f(y, \dot{y}, w(t), t) + bu, \tag{1}$$

where $f(y, \dot{y}, t)$ represents the unknown system dynamic, $w(t)$ is an unknown external disturbance, b is an unknown parameter, u is the control signal, and y is the measured output. The unknown parameter b can be represented as $b = b_0 + \tilde{b}$, where b_0 is the best available estimate of b, and $\tilde{b}$ is its associated uncertainty. By inserting this representation in (1), the following expression is obtained

$$\ddot{y} = d(t) + b_0 u(t), \tag{2}$$

where $d(t) = \tilde{b}u(t) + f(y, \dot{y}, w(t), t)$ is the total disturbance. Now, by defining the total disturbance as an extended state, $x_3 = d(t)$, the augmented state-space form of the system (2) is

$$\begin{aligned} \dot{\mathbf{x}} &= \mathbf{A}_s \mathbf{x} + \mathbf{B}_s u + \mathbf{E} h(t), \\ y &= \mathbf{C}_s \mathbf{x}, \end{aligned} \tag{3}$$

© 2011 John Wiley and Sons Asia Pte Ltd and Chinese Automatic Control Society
Prepared using asjcauth.cls

where $\mathbf{x} = \begin{bmatrix} x_1 & x_2 & x_3 \end{bmatrix}^T$ is the extended state vector with the components $x_1 = y$, $x_2 = \dot{y}$, and $x_3 = d(t)$. The system matrices are

$$\mathbf{A}_s = \begin{bmatrix} 0 & 1 & 0 \\ 0 & 0 & 1 \\ 0 & 0 & 0 \end{bmatrix}, \ \mathbf{B}_s = \begin{bmatrix} 0 \\ b_0 \\ 0 \end{bmatrix}, \ \mathbf{E} = \begin{bmatrix} 0 \\ 0 \\ 1 \end{bmatrix},$$

and $\mathbf{C}_s = \begin{bmatrix} 1 & 0 & 0 \end{bmatrix}$. The function $h(t) = \dot{d}(t)$ is the rate of change of the total disturbance, and it is assumed to be an unknown but bounded function. By treating $d(t)$ as a state, it is possible to estimate it by using the Luenberger state observer,

$$\begin{aligned} \dot{\hat{\mathbf{x}}} &= \mathbf{A}_s\hat{\mathbf{x}} + \mathbf{B}_s u + \mathbf{L}(y - \hat{y}), \\ \hat{y} &= \mathbf{C}_s\hat{\mathbf{x}}, \end{aligned} \tag{4}$$

where $\hat{\mathbf{x}} = \begin{bmatrix} \hat{x}_1 & \hat{x}_2 & \hat{x}_3 \end{bmatrix}^T$ represents the estimate of the extended state vector, and $\mathbf{L} = \begin{bmatrix} l_1 & l_2 & l_3 \end{bmatrix}^T$ is the observer gain vector. From Eq. (3) and Eq. (4) the following error equation is obtained

$$\dot{\mathbf{e}} = (\mathbf{A}_s - \mathbf{L}\mathbf{C}_s)\mathbf{e} + \mathbf{E}h, \tag{5}$$

where $\mathbf{e} = \mathbf{x} - \hat{\mathbf{x}}$. In the unperturbed case when $h = 0$, stability is determined by the characteristic equation:

$$\det(s\mathbf{I} - \mathbf{A}_s + \mathbf{L}\mathbf{C}_s) = s^3 + l_1 s^2 + l_2 s + l_3 = 0.$$

The observer gains l_1, l_2, l_3 can be calculated by the pole-placement method. By taking a stable multiple pole $-\omega_o$, where $\omega_o > 0$, from the identity $s^3 + l_1 s^2 + l_2 s + l_3 = (s + \omega_o)^3$ it follows $\mathbf{L} = \begin{bmatrix} 3\omega_o & 3\omega_o^2 & \omega_o^3 \end{bmatrix}^T$, so that the observer bandwidth, ω_o, is the only tuning parameter.

For $\omega_o > 0$, under the assumption of boundedness of $h(t)$, bounded input-bounded output stability for the observer error dynamics (5) is assured. In the special case, when the total disturbance is constant in time, $h = 0$, the estimation errors will go to zero asymptotically. Similar results can be expected if the rate of change of the total disturbance is relatively small.

The feedback control law which provides asymptotic tracking of the continuous reference signal $y_d(t)$ is $u = b_0^{-1}(\ddot{y}_d(t) - k_d\dot{\tilde{y}} - k_p\tilde{y} - d)$ so that the closed-loop tracking error $\tilde{y} = y - y_d$ satisfies $\ddot{\tilde{y}} + k_d\dot{\tilde{y}} + k_p\tilde{y} = 0$, which is asymptotically stable for the positive gains k_p and k_d. The controller gains can be determined by the pole placement method as $k_p = \omega_c^2$ and $k_d = 2\omega_c$, where ω_c is the controller bandwidth.

Usually, the velocity $\dot{y}$ and total disturbance d are not directly measured, but can be estimated using ESO (4), so that the resulting controller takes the form as

$$u = \frac{1}{b_0}[\ddot{y}_d - k_p(\hat{x}_1 - y_d) - k_d(\hat{x}_2 - \dot{y}_d) - \hat{x}_3]. \tag{6}$$

The linear ADRC has only two tuning parameters, namely, the closed-loop bandwidth ω_c and the observer bandwidth ω_o. Only observer bandwidth significantly affects the tracking speed of the ESO [14].

III. FSB ALGEBRAIC APPROACH TO ESO DESIGN

In the unperturbed case when $h = 0$, the input-output equation of the augmented state-space system (3) is

$$\dddot{y} = b_0\dot{u}(t). \tag{7}$$

The proposed FSB algebraic approach provides an estimation of the output $\hat{y}$ and its derivatives $\hat{y}^{(1)}$, and $\hat{y}^{(2)}$, based on the measured output y. The total disturbance estimate can be obtained from the Eq. (2), as $\hat{d} = \hat{y}^{(2)} - b_0 u$.

The Laplace transform of the differential equation (7) is

$$s^3 y(s) - b_0 s u(s) = R(s), \tag{8}$$

where $y(s) = \mathcal{L}\{y(t)\}$, $u(s) = \mathcal{L}\{u(t)\}$, and $R(s) = y_0 s^2 + v_0 s + a_0 - b_0 u_0$. The initial conditions $y(0) = y_0$, $\dot{y}(0) = v_0$, $\ddot{y}(0) = a_0$, and $u(0) = u_0$ are assumed to be unknown.

3.1. Annihilation of initial condition

The asymptotically convergent transient response of the conventional linear observers significantly depends on the initial conditions. The first step of the algebraic approach is the annihilation of the second-order polynomial $R(s)$, which contains unknown initial conditions. The elimination of initial conditions leads to the algebraic expressions for the estimated system states which provide nonasymptotic convergence toward its true values.

Instead of a conventional derivative-based annihilator [21], we will use the finite-difference annihilator in the complex domain [30], which leads to the stable algebraic observer realization. The finite difference operator in the Laplace domain of a function $f(s)$ is defined as follows

$$\delta_q f(s) = f(s + q) - f(s). \tag{9}$$

The difference operator decreases the order of polynomials for one degree, so that $\delta_q^n s^{n-1} = 0$. In other words, for the annihilation of the second-order polynomial function $R(s) = y_0 s^2 + v_0 s + a_0 - b_0 u_0$, the operator δ_q should be applied three times: $\delta_q R(s) = y_0(2sq + q^2) + v_0 q$, $\delta_q^2 R(s) = 2q^2 y_0$, and $\delta_q^3 R(s) = 0$.

© 2011 John Wiley and Sons Asia Pte Ltd and Chinese Automatic Control Society
Prepared using asjcauth.cls

By applying the operator δ_q^3 on (8), the following expression is obtained

$$z_3(s) - b_0 z_0(s) = 0, \tag{10}$$

where $z_0(s) = \delta_q^3[su(s)]$, and $z_3(s) = \delta_q^3[s^3 y(s)]$ can be evaluated based on definition (9),

$$\begin{aligned} z_0(s) &= (s+3q)u(s+3q) - 3(s+2q)\,(s+2q) \\ &\quad + 3(s+q)u(s+q) - su(s), \qquad (11) \\ z_3(s) &= (s+3q)^3 y(s+3q) - 3(s+2q)^3 y(s+2q) \\ &\quad + 3(s+q)^3 y(s+q) - s^3 y(s), \qquad (12) \end{aligned}$$

The equation (12) can be rearranged in the polynomial form

$$z_3(s) = s^3 w_3(s) + s^2 w_2(s) + s w_1(s) + w_0(s), \tag{13}$$

where the functions $w_i(s)$ depend linearly on the shifted values of the output $y(s+jq)$, for $i, j = 0, 1, 2, 3$. This linear relation can be represented in the matrix form

$$\mathbf{w}(s) = \mathbf{\Gamma}_1 \mathbf{y}_q(s), \tag{14}$$

where

$$\mathbf{\Gamma}_1 = \begin{bmatrix} 0 & 3q^3 & -24q^3 & 27q^3 \\ 0 & 9q^2 & -36q^2 & 27q^2 \\ 0 & 9q & -18q & 9q \\ -1 & 3 & -3 & 1 \end{bmatrix}, \tag{15}$$

and

$$\mathbf{w}(s) = \begin{bmatrix} w_0(s) \\ w_1(s) \\ w_2(s) \\ w_3(s) \end{bmatrix}, \quad \mathbf{y}_q(s) = \begin{bmatrix} y(s) \\ y(s+q) \\ y(s+2q) \\ y(s+3q) \end{bmatrix}. \tag{16}$$

Also, Eq. (11) can be rewritten in the polynomial form

$$z_0(s) = s\xi_1(s) + \xi_0(s), \tag{17}$$

where the functions $\xi_i(s)$ depend linearly on the shifted values of the input $u(s+jq)$, for $i = 0, 1$, and $j = 0, 1, 2, 3$. This linear relation can be represented in the matrix form

$$\boldsymbol{\xi}(s) = \mathbf{\Gamma}_2 \mathbf{u}_q(s), \tag{18}$$

where

$$\mathbf{\Gamma}_2 = \begin{bmatrix} 0 & 3q & -6q & 3q \\ -1 & 3 & -3 & 1 \end{bmatrix}, \tag{19}$$

and

$$\boldsymbol{\xi}(s) = \begin{bmatrix} \xi_0(s) \\ \xi_1(s) \end{bmatrix}, \quad \mathbf{u}_q(s) = \begin{bmatrix} u(s) \\ u(s+q) \\ u(s+2q) \\ u(s+3q) \end{bmatrix}. \tag{20}$$

By inserting Eqs. (13) and (17) in Eq. (10), the following polynomial expression is obtained

$$s^3 \tilde{w}_3(s) + s^2 \tilde{w}_2(s) + s\tilde{w}_1(s) + \tilde{w}_0(s) = 0, \tag{21}$$

where the functions $\tilde{w}_i(s)$, for $i = 0, 1, 2, 3$, can be expressed in the matrix form

$$\tilde{\mathbf{w}}(s) = \mathbf{w}(s) + \mathbf{T}\boldsymbol{\xi}(s), \tag{22}$$

where

$$\tilde{\mathbf{w}}(s) = \begin{bmatrix} \tilde{w}_0(s) \\ \tilde{w}_1(s) \\ \tilde{w}_2(s) \\ \tilde{w}_3(s) \end{bmatrix}, \quad \mathbf{T} = \begin{bmatrix} -b_0 & 0 \\ 0 & -b_0 \\ 0 & 0 \\ 0 & 0 \end{bmatrix}. \tag{23}$$

3.2. Invariant filtering

To overcome the effects of high-frequency noise in the measurement of the output variable we must avoid the time-derivatives of the output variable, which are represented by terms $s^j \tilde{w}_i(s) = \mathcal{L}\{\tilde{w}_i^{(j)}(t)\}$ in Eq. (21).

By multiplying (21) with $G(s)^3$, where

$$G(s) = \frac{1}{s+\lambda}, \tag{24}$$

is the low-pass invariant filter transfer function with the cut-off frequency $\lambda > 0$, we get

$$\begin{aligned} &s^3 G(s)^3 \tilde{w}_3(s) + s^2 G(s)^3 \tilde{w}_2(s) \\ &+ sG(s)^3 \tilde{w}_1(s) + G(s)^3 \tilde{w}_0(s) = 0. \end{aligned} \tag{25}$$

By using the properties of the transfer function $G(s)$

$$sG(s) = 1 - \lambda G(s), \tag{26}$$

$$s^k G(s)^n = G(s)^{n-k}[1 - \lambda G(s)]^k, \tag{27}$$

where $n = 3$ and $k = 1, 2, 3$, we can see that all time derivative operators s^k, for $k = 1, 2, 3$, can be eliminated from the expression (25). After some algebraic manipulations, the following expression is obtained

$$\tilde{w}_3(s) = G(s)\bar{w}_1(s) + G(s)^2 \bar{w}_2(s) + G(s)^3 \bar{w}_3(s), \tag{28}$$

where the complex functions $\bar{w}_i(s)$ are linearly related with the functions $\tilde{w}_j(s)$, for $i = 1, 2, 3$, and $j = 0, 1, 2, 3$. This connection can be expressed in the matrix form

$$\bar{\mathbf{w}}(s) = \mathbf{\Lambda}\tilde{\mathbf{w}}(s), \tag{29}$$

where $\bar{\mathbf{w}}(s) = \begin{bmatrix} \bar{w}_1(s) & \bar{w}_2(s) & \bar{w}_3(s) \end{bmatrix}^T$ and

$$\mathbf{\Lambda} = \begin{bmatrix} 0 & 0 & -1 & 3\lambda \\ 0 & -1 & 2\lambda & -3\lambda^2 \\ -1 & \lambda & -\lambda^2 & \lambda^3 \end{bmatrix}. \tag{30}$$

© 2011 John Wiley and Sons Asia Pte Ltd and Chinese Automatic Control Society
Prepared using asjcauth.cls

3.3. State-space realization

The expression (28) can be rearranged as

$$\tilde{w}_3(s) = G(s)\{\bar{w}_1(s) + G(s)[\bar{w}_2(s) + G(s)\bar{w}_3(s)]\},$$

and the following state variables in the complex domain can be defined

$$x_3(s) = G(s)\bar{w}_3(s), \tag{31}$$
$$x_2(s) = G(s)[\bar{w}_2(s) + x_3(s)], \tag{32}$$
$$x_1(s) = G(s)[\bar{w}_1(s) + x_2(s)], \tag{33}$$

so that

$$\tilde{w}_3(s) = x_1(s). \tag{34}$$

The state equations in the complex domain (31)-(33) can be rewritten in the time domain as

$$\dot{\mathbf{x}} = \mathbf{A}\mathbf{x} + \bar{\mathbf{w}}(t), \tag{35}$$

where

$$\mathbf{x} = \begin{bmatrix} x_1 \\ x_2 \\ x_3 \end{bmatrix}, \quad \mathbf{A} = \begin{bmatrix} -\lambda & 1 & 0 \\ 0 & -\lambda & 1 \\ 0 & 0 & -\lambda \end{bmatrix}, \tag{36}$$

and $\bar{\mathbf{w}}(t)$ is obtained from Eq. (14), (18), (22) and (29)

$$\begin{aligned} \bar{\mathbf{w}}(t) &= \mathbf{\Lambda}\tilde{\mathbf{w}}(t) = \mathbf{\Lambda}[\mathbf{w}(t) + \mathbf{T}\boldsymbol{\xi}(t)] \\ &= \mathbf{\Lambda}\mathbf{\Gamma}_1\mathbf{y}_q(t) + \mathbf{\Lambda}\mathbf{T}\mathbf{\Gamma}_2\mathbf{u}_q(t). \end{aligned} \tag{37}$$

The vector functions in the time domain $\mathbf{y}_q(t)$ and $\mathbf{u}_q(t)$ are

$$\begin{aligned} \mathbf{y}_q(t) &= \mathcal{L}^{-1}\{\mathbf{y}_q(s)\} = \boldsymbol{\varphi}(t)y(t), \\ \mathbf{u}_q(t) &= \mathcal{L}^{-1}\{\mathbf{u}_q(s)\} = \boldsymbol{\varphi}(t)u(t), \end{aligned} \tag{38}$$

where

$$\boldsymbol{\varphi}(t) = \begin{bmatrix} 1 & e^{-qt} & e^{-2qt} & e^{-3qt} \end{bmatrix}^T. \tag{39}$$

Now, the state-space equations (35) can be rewritten as

$$\dot{\mathbf{x}} = \mathbf{A}\mathbf{x} + \mathbf{b}_1(t)y(t) + \mathbf{b}_2(t)u(t), \tag{40}$$

where

$$\mathbf{b}_1(t) = \mathbf{\Lambda}\mathbf{\Gamma}_1\boldsymbol{\varphi}(t), \quad \mathbf{b}_2(t) = \mathbf{\Lambda}\mathbf{T}\mathbf{\Gamma}_2\boldsymbol{\varphi}(t), \tag{41}$$

and the output equation (34) can be written in the time domain as

$$\tilde{w}_3(t) = \mathbf{e}_1^T\mathbf{x}(t), \tag{42}$$

where $\mathbf{e}_1 = \begin{bmatrix} 1 & 0 & 0 \end{bmatrix}^T$.

3.4. Output equations

The final estimates of the system state variables, denoted as $\hat{y}^{(0)}(t)$, $\hat{y}^{(1)}(t)$, and $\hat{y}^{(2)}(t)$, will be determined from the output equation (42). The relation between function $\tilde{w}_3(t)$ and the measured system output $y(t)$ can be determined from the Eq. (14), (22), and (38)

$$\begin{aligned} \tilde{w}_3(t) &= \mathbf{e}_4^T\tilde{\mathbf{w}} = \mathbf{e}_4^T\mathbf{w} = \mathbf{e}_4^T\mathbf{\Gamma}_1\boldsymbol{\varphi}(t)y(t) \\ &= \boldsymbol{\gamma}_4^T\boldsymbol{\varphi}(t)y(t) = g(t)y(t), \end{aligned} \tag{43}$$

where $\mathbf{e}_4 = \begin{bmatrix} 0 & 0 & 0 & 1 \end{bmatrix}^T$, $\boldsymbol{\gamma}_4^T = \mathbf{e}_4^T\mathbf{\Gamma}_1 = \begin{bmatrix} -1 & 3 & -3 & 1 \end{bmatrix}$, and

$$g(t) = \boldsymbol{\gamma}_4^T\boldsymbol{\varphi}(t) = \left(e^{-qt} - 1\right)^3. \tag{44}$$

Now, by comparing the Eq. (43) with (42), we can obtain the estimate of the measured variable $y(t)$,

$$\hat{y}^{(0)}(t) = \mathbf{c}_1(t)^T\mathbf{x}, \quad \mathbf{c}_1(t)^T = \frac{1}{g(t)}\mathbf{e}_1^T. \tag{45}$$

Further, by taking the first time derivative of the Eqs. (42) and (43), the following expression is obtained

$$\begin{aligned} \dot{\tilde{w}}_3(t) &= g(t)\dot{y}(t) + \dot{g}(t)y(t) \\ &= \mathbf{e}_1^T\dot{\mathbf{x}} = \mathbf{e}_1^T\mathbf{A}\mathbf{x} + \mathbf{e}_1^T\mathbf{b}_1(t)y(t), \end{aligned} \tag{46}$$

where we used $\mathbf{e}_1^T\mathbf{b}_2(t) = 0$, so that the estimate of the first derivative can be obtained as

$$\hat{y}^{(1)}(t) = \mathbf{c}_2(t)^T\mathbf{x}, \tag{47}$$

where

$$\mathbf{c}_2(t)^T = \mathbf{c}_1(t)^T\left(-\frac{\dot{g}(t)}{g(t)}\mathbf{I} + \mathbf{A} + \mathbf{b}_1(t)\mathbf{c}_1(t)^T\right),$$

and $\mathbf{I} \in \mathbb{R}^{3\times 3}$ is the unit matrix. Following the similar procedure, the second derivative estimate of the measured variable $y(t)$ can be obtained

$$\hat{y}^{(2)}(t) = \mathbf{c}_3(t)^T\mathbf{x} + b_0u, \tag{48}$$

where we used $\mathbf{c}_1^T\mathbf{A}\mathbf{b}_2(t) = b_0$, and where

$$\begin{aligned} \mathbf{c}_3^T &= \mathbf{c}_1^T\mathbf{A}^2 + \left(-2\frac{\dot{g}(t)}{g(t)} + \mathbf{c}_1^T\mathbf{b}_1\right)\mathbf{c}_2^T \\ &+ \left(-\frac{\ddot{g}(t)}{g(t)} + \mathbf{c}_1^T\mathbf{A}\mathbf{b}_1 + \mathbf{c}_1^T\dot{\mathbf{b}}_1\right)\mathbf{c}_1^T. \end{aligned}$$

The time derivatives $\dot{g}(t)$, $\ddot{g}(t)$, and $\dot{\mathbf{b}}_1(t)$ can be calculated from the Eqs. (44), (39), and (41) as

$$\begin{aligned} \dot{g}(t) &= \boldsymbol{\gamma}_4^T\dot{\boldsymbol{\varphi}}(t) = \boldsymbol{\gamma}_4^T\mathbf{\Upsilon}\boldsymbol{\varphi}(t), \\ \ddot{g}(t) &= \boldsymbol{\gamma}_4^T\mathbf{\Upsilon}\dot{\boldsymbol{\varphi}}(t) = \boldsymbol{\gamma}_4^T\mathbf{\Upsilon}^2\boldsymbol{\varphi}(t), \\ \dot{\mathbf{b}}_1(t) &= \mathbf{\Lambda}\mathbf{\Gamma}_1\mathbf{\Upsilon}\boldsymbol{\varphi}(t), \end{aligned} \tag{49}$$

© 2011 John Wiley and Sons Asia Pte Ltd and Chinese Automatic Control Society
Prepared using asjcauth.cls

where $\dot{\boldsymbol{\varphi}}(t) = \boldsymbol{\Upsilon}\boldsymbol{\varphi}(t)$, and $\boldsymbol{\Upsilon} = \text{diag}\{0, -q, -2q, -3q\}$.

Finally, the vector of estimated states can be written as

$$\hat{\mathbf{y}}(t) = \mathbf{C}(t)\mathbf{x}, \tag{50}$$

where $\hat{d}(t) = \hat{y}^{(2)}(t) - b_0 u(t)$, and

$$\hat{\mathbf{y}}(t) = \begin{bmatrix} \hat{y}^{(0)}(t) \\ \hat{y}^{(1)}(t) \\ \hat{d}(t) \end{bmatrix}, \quad \mathbf{C}(t) = \begin{bmatrix} \mathbf{c}_1(t)^T \\ \mathbf{c}_2(t)^T \\ \mathbf{c}_3(t)^T \end{bmatrix}. \tag{51}$$

The singularity of the matrix $\mathbf{C}(t)$ in the time instant $t = 0$ can be avoided by the evaluation in $t \geq \varepsilon > 0$, where ε is some small positive parameter, [22, 31].

3.5. ADRC based on algebraic ESO

The ADRC based on algebraic ESO has the same form as the ADRC based on linear ESO (6), with $\hat{x}_1 = \hat{y}^{(0)}$, $\hat{x}_2 = \hat{y}^{(1)}$, and $\hat{x}_3 = \hat{d}$. In the matrix formulation, the control low (6) can be rewritten as

$$u = \frac{1}{b_0}\mathbf{k}^T(\mathbf{y}_d(t) - \hat{\mathbf{y}}(t)), \tag{52}$$

where

$$\mathbf{k} = \begin{bmatrix} k_p & k_d & 1 \end{bmatrix}^T, \quad \mathbf{y}_d(t) = \begin{bmatrix} y_d(t) & \dot{y}_d(t) & \ddot{y}_d(t) \end{bmatrix}^T.$$

The overall closed-loop control system is illustrated in Fig. 1.

IV. COMPARISON WITH LINEAR ESO

In this section, the asymptotic equivalence between algebraic and linear ESO is proven in the case when $\lambda = \omega_o$. This equivalence provides a framework for an adequate comparison of the algebraic and linear ESO.

4.1. Asymptotic equivalence with Luenberger observer

In the asymptotic case when $t \to \infty$, we have

$$\bar{\boldsymbol{\varphi}} = \lim_{t\to\infty} \boldsymbol{\varphi}(t) = \begin{bmatrix} 1 & 0 & 0 & 0 \end{bmatrix}^T,$$

$$\bar{\mathbf{b}}_1 = \lim_{t\to\infty} \mathbf{b}_1(t) = \boldsymbol{\Lambda}\boldsymbol{\Gamma}_1\bar{\boldsymbol{\varphi}} = \begin{bmatrix} -3\lambda & 3\lambda^2 & -\lambda^3 \end{bmatrix}^T,$$

$$\bar{\mathbf{b}}_2 = \lim_{t\to\infty} \mathbf{b}_2(t) = \boldsymbol{\Lambda}\mathbf{T}\boldsymbol{\Gamma}_2\bar{\boldsymbol{\varphi}} = b_0 \begin{bmatrix} 0 & -1 & \lambda \end{bmatrix}^T,$$

$$\bar{\mathbf{C}} = \lim_{t\to\infty} \mathbf{C}(t) = \begin{bmatrix} -1 & 1 & 0 \\ -2\lambda & -1 & 1 \\ \lambda^2 & -\lambda & -1 \end{bmatrix},$$

so that the linear time-varying state-space and output equations (40) and (50) become the linear time invariant equations

$$\dot{\boldsymbol{x}} = \mathbf{A}\boldsymbol{x} + \bar{\mathbf{b}}_1 y(t) + \bar{\mathbf{b}}_2 u(t), \quad \hat{\boldsymbol{y}} = \bar{\mathbf{C}}\boldsymbol{x}. \tag{53}$$

Now, by inserting the state vector obtained from the output equation, $\boldsymbol{x} = \bar{\mathbf{C}}^{-1}\hat{\boldsymbol{y}}$, in the state-space equation, the following expression is obtained

$$\dot{\hat{\boldsymbol{y}}} = \bar{\mathbf{C}}\mathbf{A}\bar{\mathbf{C}}^{-1}\hat{\boldsymbol{y}} + \bar{\mathbf{C}}\bar{\mathbf{b}}_1 y(t) + \bar{\mathbf{C}}\bar{\mathbf{b}}_2 u(t). \tag{54}$$

The linear ESO state-space equation (4) can be rewritten in the form

$$\dot{\hat{\mathbf{x}}} = (\mathbf{A}_s - \mathbf{L}\mathbf{C}_s)\hat{\mathbf{x}} + \mathbf{L}y + \mathbf{B}_s u. \tag{55}$$

By comparing the Eq. (54) with (55) in the case when $\omega_o = \lambda$, it follows

$$\bar{\mathbf{C}}\mathbf{A}\bar{\mathbf{C}}^{-1} = \mathbf{A}_s - \mathbf{L}\mathbf{C}_s = \begin{bmatrix} -3\lambda & 1 & 0 \\ -3\lambda^2 & 0 & 1 \\ -\lambda^3 & 0 & 0 \end{bmatrix}, \tag{56}$$

$$\bar{\mathbf{C}}\bar{\mathbf{b}}_1 = \mathbf{L} = \begin{bmatrix} 3\lambda & 3\lambda^2 & \lambda^3 \end{bmatrix}^T, \tag{57}$$

$$\bar{\mathbf{C}}\bar{\mathbf{b}}_2 = \mathbf{B}_s = \begin{bmatrix} 0 & b_0 & 0 \end{bmatrix}^T. \tag{58}$$

In other words, the algebraic ESO, in the asymptotic case when $t \to \infty$ and $\omega_o = \lambda$, is equivalent to the linear ESO.

4.2. Comparison of algebraic and linear ESO

The main characteristics of the linear and algebraic ESO are summarized in Table 1. The FSB algebraic approach to the ESO design leads to the linear time-varying state-space realization which provides nonasymptotic convergence of the estimated states. This almost instantaneous convergence toward exact values of the system states and total disturbance resolves several problems of the linear ESO: a) the peaking phenomenon; b) the transient response sensitivity on the observer bandwidth ω_o; c) noise amplification due to the high gain observer design.

The ADRC based on linear ESO guarantees good tracking performances only in the case when the observer bandwidth ω_o is much higher than the controller bandwidth ω_c, $\omega_o \gg \omega_c$. But, the high value of ω_o leads to the measurement noise amplification, and the peaking phenomenon becomes more enhanced.

On the other side, the nonasymptotic convergence of the algebraic ESO does not depend on the observer bandwidth λ, which means that the transient response

© 2011 John Wiley and Sons Asia Pte Ltd and Chinese Automatic Control Society
Prepared using asjcauth.cls

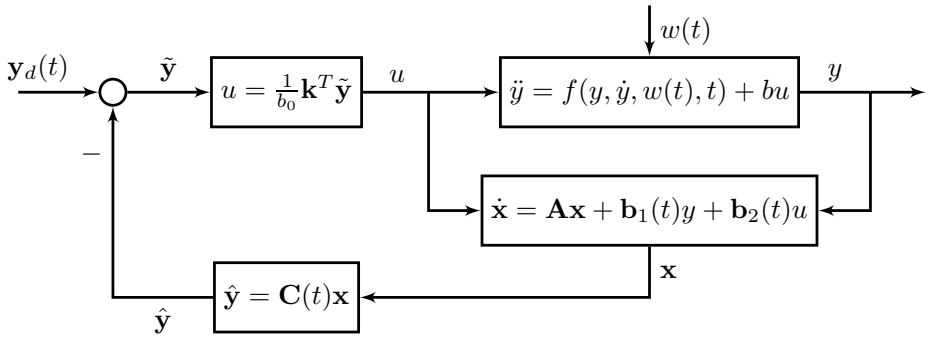

Fig. 1. The block diagram of ADRC based on algebraic ESO.

Table 1. Comparison of the main characteristics of the linear and algebraic ESO in the case of constant or slow varying disturbances.

	Linear ESO	Algebraic ESO
State-space realization	$\dot{\hat{\mathbf{x}}} = \mathbf{A}_s\hat{\mathbf{x}} + \mathbf{B}_s u + \mathbf{L}(y - \hat{y})$ $\hat{y} = \mathbf{C}_s\hat{\mathbf{x}}$	$\dot{\mathbf{x}} = \mathbf{A}\mathbf{x} + \mathbf{b}_1(t)y + \mathbf{b}_2(t)u$ $\hat{\mathbf{y}} = \mathbf{C}(t)\mathbf{x}$
Estimation convergence	asymptotic; dependent on initial conditions	nonasymptotic; independent on initial conditions
Peaking phenomenon	inevitable, especially for large values of ω_o	eliminated; independent on parameters λ and q
Transient response	depends on ω_c and ω_o; good response only for $\omega_o \gg \omega_c$	depends only on ω_c; good response even for $\lambda < \omega_c$
Noise attenuation	amplify noise because of high value of $\omega_o \gg \omega_c$	suppress noise because of low value of $\lambda < \omega_c \ll \omega_o$

of ADRC based on algebraic ESO depends only on controller bandwidth ω_o. Also, for the low values of the observer bandwidth, $\lambda < \omega_c \ll \omega_o$, the algebraic ESO is much less sensitive to the measurement noise in comparison with linear ESO.

The mentioned characteristics of the linear and algebraic extended state observers will be illustrated by simulation examples in the subsequent section.

V. SIMULATION RESULTS

In this section, the performances of the FSB algebraic ESO are compared with the conventional linear ESO. The first example illustrates the elimination of the peaking phenomenon in the case of the algebraic ESO. The second example illustrates the low sensitivity of the closed-loop system response regarding the choice of the observer bandwidth. Simulation results are obtained by using Matlab 4th order Runge-Kutta integration routine.

5.1. DC servo motor motion control

The dynamic model of the Quanser's DC servo motor motion control system, presented in [12], is

$$\dot{x}_1 = x_2, \qquad \dot{x}_2 = ax_2 + bu, \tag{59}$$

where the state variables are $x_1 = \theta$ and $x_2 = \dot{\theta}$, θ is motor load angle, u is the motor control voltage, the output variable is $y = x_1$, $a = -((B_{eq}R_m + \eta_g\eta_m K_m K_t K_g^2)/(J_{eq}R_m))$, and $b = (\eta_g\eta_m K_t K_g)/(J_{eq}R_m))$. The parameter B_{eq} is the viscous damping coefficient, R_m is the armature resistance, η_g is the gearbox efficiency, η_m is the motor efficiency, K_m is the back EMF constant, K_t is the motor torque constant, K_g is the gearbox ratio and J_{eq} is equivalent moment of inertia at the load.

The nominal values of system parameters, including the controller and observer gains, are also taken from [12]. The system parameters are: $B_{eq} = 0.004$ Nm/(rad/s), $R_m = 2.6\ \Omega$, $\eta_g = 0.9$, $\eta_m = 0.69$,

© 2011 John Wiley and Sons Asia Pte Ltd and Chinese Automatic Control Society
Prepared using asjcauth.cls

$K_m = 0.00767$ V/(rad/s), $K_t = 0.00767$ Nm, and $K_g = 70$ and $J_{eq} = 0.0021$ kg m^2. The controller gains are obtained for the controller bandwidth $\omega_c = 10$ rad/s. The gains of the linear ESO are obtained for the observer bandwidth $\omega_o = 60$ rad/s. The reference signal is $\theta_d = \sin(t)$.

In [12], the initial conditions for the plant, as well as observer, are taken as zero. In this simulation example, the nonzero plant initial conditions are chosen, $\theta(0) = 0.5$ rad and $\dot{\theta}(0) = -0.3$ rad/s, with aim to illustrate the peaking phenomenon.

Since the algebraic ESO in asymptotic case is equivalent with linear ESO, the parameter λ is chosen same as the linear ESO observer bandwidth, $\lambda = \omega_o = 60$ rad/s. The switch-on time of the algebraic ESO is $\epsilon = 0.02$ s, and the frequency shift is $q = 0.1$.

The comparison between linear and algebraic ESO is shown in Figs. 2-6. It can be seen from Fig. 2 that estimated positions have a similar response. But, the estimated velocity in the case of linear ESO has a high amplitude transient in a short initial time interval, as can be seen in Fig. 3. The maximal value of the estimated velocity is 18.27 rad/s for the linear ESO, and 1.03 rad/s for the algebraic ESO. This high amplitude transient is a typical manifestation of the peaking phenomenon, as a consequence of the nonzero initial conditions and the high observer gains. The velocity estimation error $\hat{y}^{(1)} - y^{(1)}$ for the linear and algebraic ESO is shown in Fig. 4. It can be seen that the estimation error is much larger in the case of linear ESO. The small velocity error of the algebraic ESO is a direct consequence of the nonasymptotic convergence.

For the linear ESO, the peaking phenomenon is especially dominant in the case of disturbance estimate, as it is shown in Fig. 5. The maximal value of the estimated disturbance is 416.84 for the linear ESO, and 53.82 for the algebraic ESO. The observed peaking phenomenon in the case of linear ESO has as a consequence the high amplitude peak of the control variable, as illustrated in Fig. 6. On the other hand, the algebraic ESO provides a very fast estimation of the velocity and total disturbance, without any overshoots.

The numerical results in Table 2 provide a comparison of the maximal values of estimated variables for the linear and algebraic ESO for different choices of the initial conditions. It can be seen that the maximal values of estimated variables are much larger in the case of the linear ESO, which is a direct consequence of the peaking phenomenon.

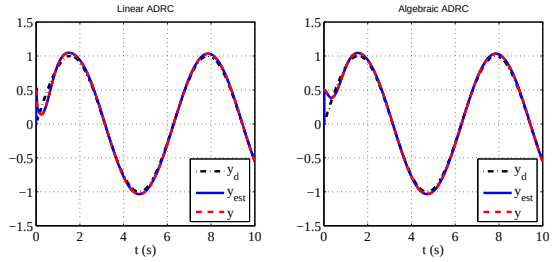

Fig. 2. The estimated positions for the linear and algebraic ESO.

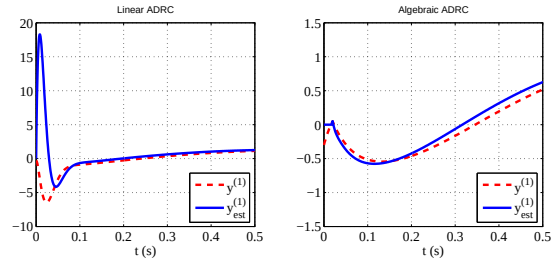

Fig. 3. The estimated velocities for the linear and algebraic ESO.

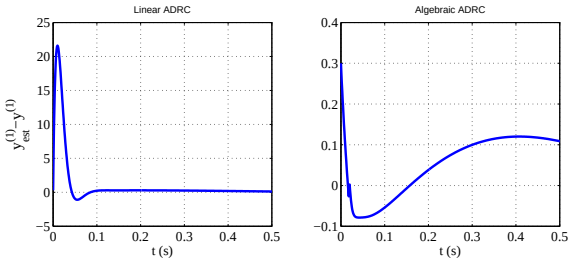

Fig. 4. The velocities estimation error for the linear and algebraic ESO.

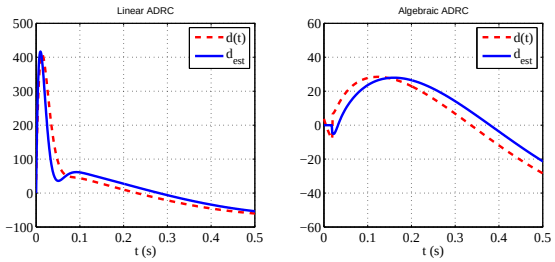

Fig. 5. The estimated disturbances for the linear and algebraic ESO.

5.2. Multirotor altitude control

The altitude dynamics of a multirotor [31] can be reduced to

$$m\ddot{z} = -mg + d_{ext} + u, \tag{60}$$

© 2011 John Wiley and Sons Asia Pte Ltd and Chinese Automatic Control Society
Prepared using asjcauth.cls

Table 2. Estimated values of system parameters in the cases with and without measurement noise.

		Linear ESO			Algebraic ESO		
$y(0)$	$\dot{y}(0)$	$\max\|\hat{y}^{(1)}(t)\|$	$\max\|\hat{d}(t)\|$	$\max\|u(t)\|$	$\max\|\hat{y}^{(1)}(t)\|$	$\max\|\hat{d}(t)\|$	$\max\|u(t)\|$
0.0	0.0	1.205	61.365	0.673	1.134	58.353	0.639
0.5	0.0	18.340	418.40	8.830	1.037	53.824	0.588
0.5	−0.3	18.277	416.84	8.798	1.037	53.826	0.588
−0.5	0.0	18.039	418.75	9.215	2.494	126.63	1.398
−0.5	0.3	17.985	417.19	9.182	2.481	126.02	1.391

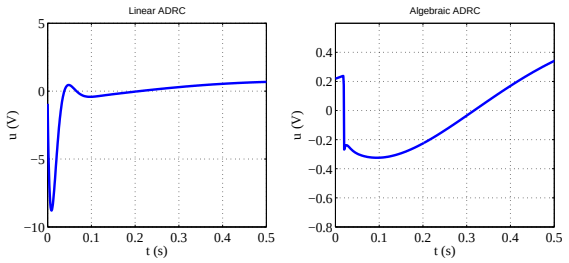

Fig. 6. The control signals for the linear and algebraic ESO.

where m is the multirotor mass, g is the gravity constant, u is the control thrust force, and d_{ext} is the external disturbance like unknown slow varying wind force or unknown constant lifting force in the case of the balloon-quadrotor. The Eq. (60) can be rewritten as $\ddot{z} = b_0 u + d$, where b_0 is the best estimate of the parameter $b = 1/m$, and the total disturbance is $d = (b - b_0)u + (d_{ext} - mg)/m$. The nominal values of parameters are taken as $m = 0.5$ kg, and $d_{ext} = 10.9$ N.

In this example, the controller bandwidth is relatively low, $\omega_c = 1$, and Fig. 7 and Fig. 8 illustrate the closed-loop responses for the linear and algebraic ESO. The parameter b_0 is chosen as $b_0 = b$, so that the total disturbance is the unknown constant acceleration, $d = d_{ext}/m - g$. It can be seen that the response of the system in the closed loop with the linear ESO significantly depends on the choice of the observer bandwidth ω_o. In the case of linear ESO, the satisfactory system response without overshoots can be achieved for the higher values of the observer bandwidth. On the other hand, the response of the system in the closed loop with the algebraic ESO is invariant to the choice of the observer bandwidth λ, and depends only on the choice of the controller bandwidth ω_c. Since the choice of the observer bandwidth λ has no influence on the system response, it can be chosen low enough to reduce noise sensitivity of the observer.

Figures 9 and 10 illustrate the performances of the linear and algebraic ESO in the case of the position measurement noise, $z_m(t) = z(t) + 0.8\chi(t)$, where $\chi(t)$ is some Gaussian noise of standard normal distribution $\mathcal{N}(0, 1)$. Fig. 9 shows the closed-loop response in the case of algebraic ESO for the choice $\lambda = 1$, and a similar response in the case of linear ESO, obtained for $\omega_o = 7$. Fig. 10 shows the total disturbance estimates in the case of the linear and algebraic ESO. It can be seen that possibility of choosing small values of the observer bandwidth in the case of algebraic ESO provides significant noise reduction in comparison with the linear ESO.

Figures 11 and 12 illustrate the closed-loop responses and disturbance estimate in the case when $b_0 = 2b$. In this case, the total disturbance is time-varying since it depends on the control variable. It can be seen that the convergence of the algebraic ESO is not almost instantaneous, as in the case of the constant total disturbance. But, it is still much faster than in the case of linear ESO. The fast disturbance estimation provides a closed-loop system response with much smaller overshoots than in the case of linear ESO.

VI. EXPERIMENTAL RESULTS

In order to verify the simulation results, a two-rotor experimental setup was designed and manufactured. The setup consists of two quadrotor arms, the central part and the axis around which the rotor arms rotate, where the control of the pitch angle is considered. The rotor arms are 200 mm long, at the ends of which are mounted propulsion units which consist of an MN2214 (920 Kv) BLDC motor on which a Graupner cProp 9040 propeller is mounted, and the motor is

© 2011 John Wiley and Sons Asia Pte Ltd and Chinese Automatic Control Society
Prepared using asjcauth.cls

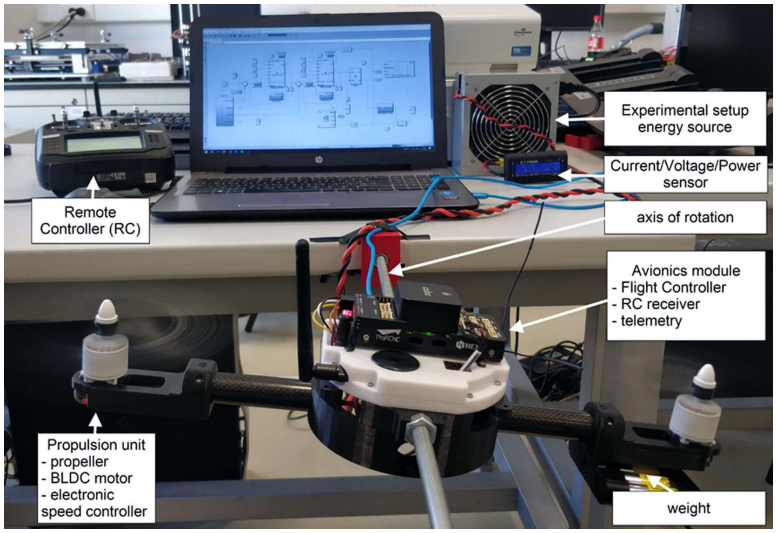

Fig. 13. The experimental setup.

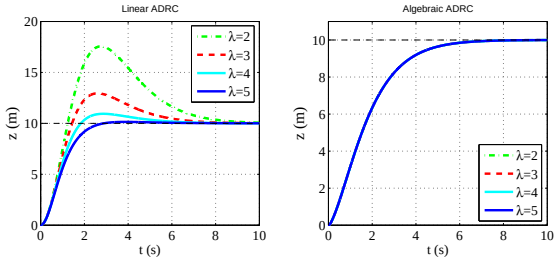

Fig. 7. The response of the system in closed-loop with the linear and algebraic ESO, in the case when $b_0 = b$, and $\omega_o = \lambda$.

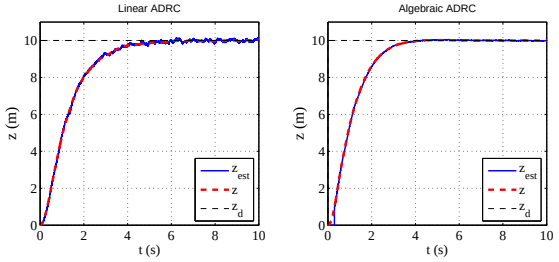

Fig. 9. The closed-loop system response of the linear ESO with $\omega_o = 7$, and algebraic ESO with $\lambda = 1$, in the case with measurement noise.

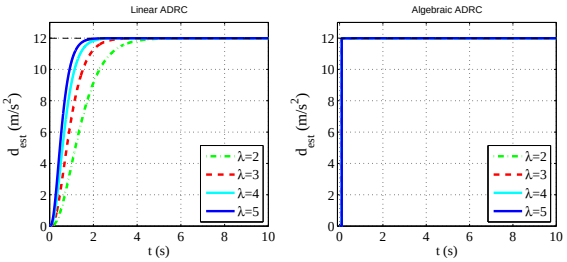

Fig. 8. The total disturbance estimate for the linear and algebraic ESO, in the case when $b_0 = b$, and $\omega_o = \lambda$.

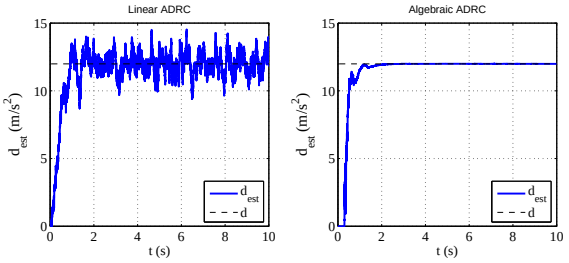

Fig. 10. The total disturbance estimate of the linear ESO with $\omega_o = 7$, and algebraic ESO with $\lambda = 1$, in the case with measurement noise.

controlled by KW30E ESC. The control system consists of a Pixhawk Cube flight controller with an associated remote control module. The control algorithm was written and implemented using Matlab Simulink, in which a connection with the experimental setup is achieved in real-time using external communication.

For testing purposes, a load of mass $m_1 = 0.12$ kg was placed on one arm, at a distance of $d_1 = 0.16$ m from the center of rotation. The experimental setup is shown in Fig. 13.

© 2011 John Wiley and Sons Asia Pte Ltd and Chinese Automatic Control Society
Prepared using asjcauth.cls

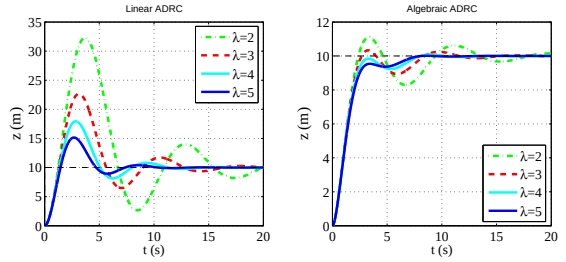

Fig. 11. The response of the system in closed-loop with the linear and algebraic ESO, in the case when $b_0 = 2b$, and $\omega_o = \lambda$.

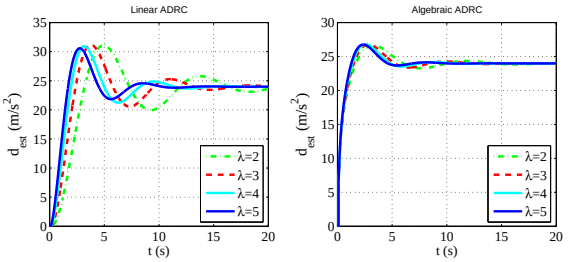

Fig. 12. The total disturbance estimate for the linear and algebraic ESO, in the case when $b_0 = 2b$, and $\omega_o = \lambda$.

The angular dynamics of the two-rotor system with the load can be written as

$$J\ddot{\theta} = -m_1 d_1 g \cos(\theta) + u, \qquad (61)$$

where J is the two-rotor moment of inertia, g is the gravity constant, θ is the angular position, and u is the control torque. The Eq. (61) can be rewritten as $\ddot{\theta} = b_0 u + d$, where b_0 is the best estimate of the parameter $b = 1/J$, and the total disturbance is $d = (b - b_0)u - m_1 d_1 g \cos(\theta)/J$. The initial conditions are $\theta(0) = -0.58$ rad and $\dot{\theta}(0) = 0$ rad/s.

The linear and algebraic ESO are used for the monitoring of the system state and disturbance. Fig. 14 shows the measured angular position and control torque, which are used as inputs for the observers. The parameter λ of the algebraic ESO is chosen same as the linear ESO observer bandwidth, $\lambda = \omega_o = 8$ rad/s. The switch-on time of the algebraic ESO is $\epsilon = 0.1$ s, and the frequency shift is $q = 0.2$.

The estimated angular position, velocity and total disturbance, for the linear and algebraic ESO, are shown in Figs. 15-17. It can be seen that the estimated velocity and total disturbance in the case of linear ESO have a large initial estimation error. On the other hand, the algebraic ESO eliminates the initial peaking of the estimated variables. After some transient time, the estimated variables of both observers look very similar, as can be expected from the asymptotic equivalence of the linear and algebraic ESO.

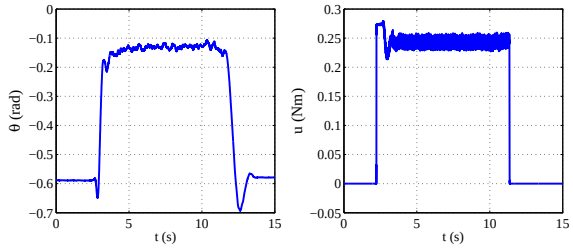

Fig. 14. The measured angular position and control torque.

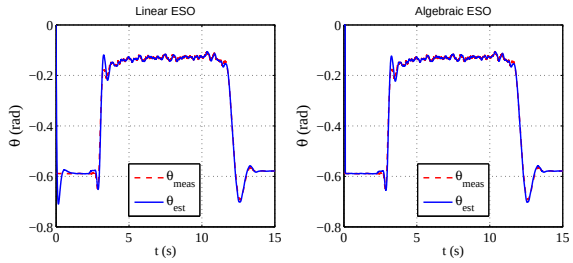

Fig. 15. The angular position estimate for the linear and algebraic ESO.

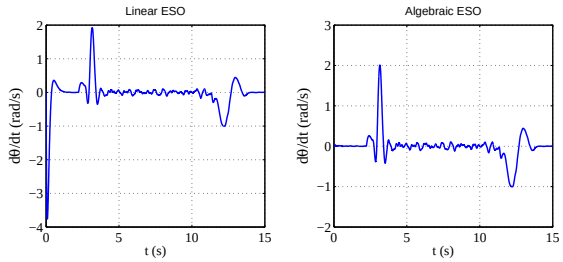

Fig. 16. The angular velocity estimate for the linear and algebraic ESO.

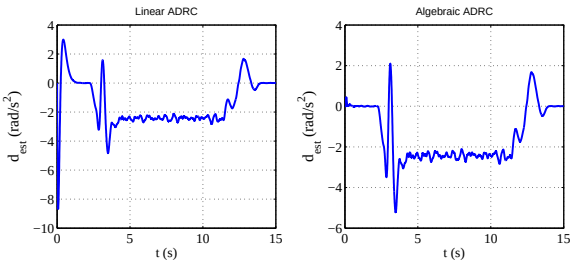

Fig. 17. The total disturbance estimate for the linear and algebraic ESO.

© 2011 John Wiley and Sons Asia Pte Ltd and Chinese Automatic Control Society
Prepared using asjcauth.cls

VII. CONCLUSIONS

In this paper, a new stable algebraic approach to the extended state observer has been proposed. The proposed algebraic ESO provides nonasymptotic convergence toward the exact values of the state variables, ensuring the elimination of the peaking phenomenon. The nonasymptotic convergence of the algebraic ESO provides a closed-loop system response that is less sensitive to the choice of the observer bandwidth. In the case of constant or slow-varying disturbances, the bandwidth of the algebraic ESO can be chosen enough small to reduce the influence of the measurement noise, without deterioration of the closed-loop system response. The future work will be oriented toward FSB algebraic design of the generalized ESO with the arbitrary number of extended states, which will provides better estimation accuracy in the case of the fast time-varying disturbances.

Acknowledgment

This work has been supported by European Regional Development Fund, Operational programme competitiveness and cohesion 2014-2020, grant number KK.01.1.1.04.0092.

REFERENCES

1. Gao, Z., "Active Disturbance Rejection Control: A Paradigm Shift in Feedback Control System Design", *Proc. of the 2006 American Control Conference*, Minneapolis, USA, June 14-16, pp. 2399-2405 (2006).
2. Han, J., "From PID to Active Disturbance Rejection Control", *IEE Transaction on Industrial Electronics*, Vol. 56, No. 3, pp. 900-906 (2009).
3. Guo, B.-Z., and Z.-L. Zhao, *Active Disturbance Rejection Control for Nonlinear Systems: An Introduction*, John Wiley & Sons, Singapore (2016).
4. Gao, Z., "On the centrality of disturbance rejection in automatic control", *ISA Transactions*, Vol. 53, No. 4, pp. 850-857 (2014).
5. Chen, W-H., Yang, J., Guo, L., and S. Li, "Disturbance Observer-Based Control and Related Methods: An Overview", *IEEE Transactions on Industrial Electronics*, Vol. 63, No. 2, pp. 1083-1095 (2015).
6. Kuang, Z., Du, B., Cui, S. and Chan, C. C., "Speed Control of Load Torque Feedforward compensation based on Liner Active Disturbance Rejection for Five-Phase PMSM", *IEEE Access*, Vol. 7, pp. 159787-159796 (2019).
7. Rosas Almeida, D. I., Alvarez, J., and Cantu Cardenas, J. A., "Application of the active disturbance rejection control structure to improve the controller performance of uncertain pneumatic actuators", *Asian Journal of Control*, Vol. 21, No. 1, pp. 99-113 (2019).
8. Sun, H., Sun, Q., Wu, W., Chen, Z., and J. Tao, "Altitude control for flexible wing unmanned aerial vehicle based on active disturbance rejection control and feedforward compensation", *International Journal of Robust and Nonlinear Control*, Vol. 30, No. 1, pp. 222-245 (2020).
9. Morales, R., Sira-Ramrez, H., and J. A. Somolinos, "Linear active disturbance rejection control of the hovercraft vessel model", *Ocean Engineering*, Vol. 96, pp. 100-108 (2015).
10. Ran, M., Wang, Q., Dong, S., and Xie, L., "Active disturbance rejection control for uncertain time-delay nonlinear systems", *Automatica*, Vol. 112, p. 108692 (2020).
11. Madonski, R., and P. Herman, "Survey on methods of increasing the efficiency of extended state disturbance observers," *ISA Transactions*, Vol. 56, pp. 18-27 (2015).
12. Godbole, A. A., Kolhe, J. P., and S. E. Talole, "Performance Analysis of Generalized Extended State Observer in Tackling Sinusoidal Disturbances," *IEEE Transactions on Control Systems Technology*, Vol. 21, No. 6, pp. 2212-2223 (2013).
13. Ahi, B., and Haeri, M., "Linear Active Disturbance rejection Control from the Practical Aspects", *IEEE/ASME Transactions on Mechatronics*, Vol. 23, No. 6, pp. 2909-2919 (2018).
14. Yoo, D., Yau, S. S.-T. and Z. Gao, "Optimal fast tracking observer bandwidth of the linear extended state observer", *International Journal of Control*, Vol. 80, No. 1, pp. 102-111 (2007).
15. Astolfi, D., Marconi, L. and Teel, A., "Lower-power peaking-free high-gain observers for nonlinear systems," *2016 European Control Conference (ECC)*,(2016).
16. Teel, A. R., "Further variants of the Astolfi/Marconi high-gain observer," *2016 American Control Conference (ACC)* (2016).
17. Khalil, H. K., "Cascade high-gain observers in output feedback control," *Automatica*, Vol. 80, pp. 110-118 (2017).
18. Wu, Z., Huang, G., Wu, C., Lv, C., Bao, L., "On convergence of extended state observer for a class of MIMO uncertain stochastic nonlinear systems," *IEEE Access*, Vol. 6, pp. 37758-37766 (2018).

© 2011 John Wiley and Sons Asia Pte Ltd and Chinese Automatic Control Society
Prepared using asjcauth.cls

19. Zhao, Z.-L., Guo, B.-Z., "A novel extended state observer for output tracking of MIMO systems with mismatched uncertainty," *IEEE Transactions on Automatic Control*, Vol. 63, No. 1, pp. 211-218 (2017).
20. Barreiro, A., and E. Delgado, "Reset observers alleviating the peaking and the robustness trade-offs: A case study on force estimation in teleoperation," *ISA Transactions*, Vol. 94, pp. 36-46 (2019).
21. Fliess, M., and H. Sira-Ramírez, "An algebraic framework for linear identification," *ESAIM Control Optimisation and Calculus of Variations*, Vol. 9, pp. 151-168 (2003).
22. Sira-Ramírez, H., C. G. Rodríguez, J. C. Romero, and A. L. Juárez, *Algebraic Identification and Estimation Methods in Feedback Control Systems*, John Wiley & Sons, Chichester, West Sussex (2014).
23. Delpoux, R., and T. Floquet, "On-line parameter estimation via algebraic method: An experimental illustration", *Asian Journal of Control*, Vol. 17, No. 1, pp. 315-326 (2015).
24. Beltran-Carbajal, F. and G .Silva-Navarro, "Generalized nonlinear stiffness identification on controlled mechanical vibrating systems," *Asian Journal of Control*, Vol. 21, No. 4, pp. 1281-1292 (2019).
25. Fliess, M., and H. Sira-Ramírez, "State reconstructors: a possible alternative to asymptotic observers and Kalman filters," *Proceedings CESA 2003*, Lille, France (2003).
26. Fliess, M., C. Join, and H. Sira-Ramírez, "Nonlinear estimation is easy," *Int. J. Modelling Identification and Control*, Vol. 4, pp. 12-27 (2008).
27. Mamani, G., J. Becedas, V. Feliu-Batlle, and H. Sira-Ramirez, "Algebraic Observers to Estimate Unmeasured State Variables of DC Motors," *Engineering Letters*, Vol. 16, (2008).
28. Mboup, M., C. Join, and M. Fliess, "Numerical differentiation with annihilators in noisy environment," *Numerical Algorithms*, Vol. 50, pp. 439-467 (2009).
29. Morales, R., E. Segura, J. A. Somolinos, L. R. Núñez, and H. Sira-Ramírez, "Online signal filtering based on the algebraic method and its experimental validation," *Mechanical Systems and Signal Processing*, Vol. 66-67, pp. 374-387 (2016).
30. Kasac, J., T. Zilic, V. Milic, and A. Jokic, "Frequency-shifting-based stable on-line algebraic parameter identification of linear systems," *Journal of the Franklin Institute*, Vol. 355, No. 18, pp. 9224-9244 (2018).
31. Kasac, J., Kotarski, D., and P. Piljek, "Frequency-shifting based algebraic approach to stable on-line parameter identification and state estimation of multirotor UAV," *Asian Journal of Control*, Vol. 21, No. 4, pp. 1619-1629 (2019).
32. Kasac, J., Majetic, D., and D. Brezak, "An algebraic approach to on-line signal denoising and derivatives estimation," *Journal of the Franklin Institute*, Vol. 355, No. 15, pp. 7799-7825 (2018).

Josip Kasac is a professor in the Department of Robotics and Automation of Manufacturing Systems at Faculty of Mechanical Engineering and Naval Architecture, University of Zagreb, Croatia. Dr. Kasac received his Ph.D. in Mechanical Engineering from the University of Zagreb in 2005. His research interests are control of nonlinear mechanical systems, optimal control and algebraic estimation methods.

Antonia Pender received her Master's degree in Mechanical Engineering from The University of Zagreb in 2017. She is a Ph.D. candidate in the Department of Robotics and Automation of Manufacturing Systems at Faculty of Mechanical Engineering and Naval Architecture, University of Zagreb, Croatia. She is currently an assistant in the Mechanical Engineering department of Zagreb University of Applied Sciences, Croatia. Her research interests include algebraic estimation methods and nonlinear control design.

Marko Pranjic received his Master's degree in Mechanical Engineering from the University of Zagreb in 2019. He is a research assistant in the Department of Mechanical Engineering at Karlovac University of Applied Sciences, Croatia. His research interests include nonlinear control design, and control algorithm implementations.

© 2011 John Wiley and Sons Asia Pte Ltd and Chinese Automatic Control Society
Prepared using asjcauth.cls

Denis Kotarski is a lecturer in the Department of Mechanical Engineering at Karlovac University of Applied Sciences, Croatia. He received his Ph.D. in Mechanical Engineering from the University of Zagreb in 2020. His research interests include multirotor UAV design and robust control.

© 2011 John Wiley and Sons Asia Pte Ltd and Chinese Automatic Control Society
Prepared using asjcauth.cls